Fast defect detection in textured surfaces using 1D Gabor filters

D. M. Tsai and C. P. Lin
Machine Vision Lab.
Department of Industrial Engineering and Management
Yuan-Ze University, Chung-Li, Taiwan, R.O.C.
E-mail: iedmtsai@saturn.yzu.edu.tw

Abstract

In this paper, we present a fast machine vision method for the automatic inspection of defects in textured surfaces. Traditional 2D Gabor filtering schemes have shown to be very effective for detecting local anomalies in textured surfaces of industrial materials. However, they are computationally expensive and sensitive to image rotation. In order to alleviate the limitations of 2D Gabor filtering, we first use the 1D ring-projection transformation to compress a 2D gray-level image to a 1D pattern, and then employ a 1D Gabor filter to detect defects embedded in a homogeneous texture. Given a problem with image size $N \times N$ and filter window $W \times W$, the computational complexity can be significantly reduced from $O(W^2N^2)$ in the 2D Gabor space to $O(WN^2)$ in the 1D Gabor space, and the detection results are invariant to rotation changes of a texture. The experiments on structural textures such as wooden surface, LCD display and machined surface, and statistical textures such as granite, leather and sandpaper have shown the efficiency and effectiveness of the proposed method.

Keywords: Defect detection; Machine vision; 1D Gabor filter; Ring projection; Surface inspection

1. Introduction

Visual inspection makes up an important part of quality control in manufacturing. The manual activity of inspection could be subjective and highly dependent on the experience of human inspectors. In this study, we propose a fast machine vision method for automatic surface inspection.

In automatic surface inspection, small defects that locally break the homogeneity of a textured surface must be detected. The surfaces of many industrial materials have textural appearance in images. Textures are generally classified into two major types, structural and statistical [1]. Structural textures are those that are composed of repetitions of some basic texture primitives, such as lines, with deterministic rules of displacement. This type of textures arises in textile fabrics, machined surfaces, patterned wafers, LCD displays, CCD arrays, and the surfaces of many man-made products. Structural textures generally show oriented patterns on the surface and, therefore, their appearances in rotated images are different. Statistical textures cannot be described with texture primitives and deterministic displacement rules. The spatial distribution of gray levels in such a textured image is rather stochastic. Sandpaper, leather, and many metallic surfaces under the magnification of microscopes fall in this category. Statistical textures generally show isotropic patterns on the surface and, therefore, their appearances are invariant to image rotation. Defect detection in both structural and statistical textures is studied in this paper.

The inspection task in this paper is classified as qualitative inspection [2] which involves detecting novel but obviously fault items such as scratches, cracks, stains and other ill-defined flaws. Many of these unanticipated defects are small in size, and cannot be described by quantifiable measures, making automatic defect detection in textured surfaces difficult.

In the recent past, Gabor filters [3, 4] have been well recognized as a joint spatial/spatial-frequency representation for analyzing textured images containing highly specific frequency and orientation characteristics. Daugman [5] showed that Gabor filters have optimal joint localization in both the spatial and the spatial-frequency domains. Compared to the Fourier transform that only characterizes the spatial-frequency in a global approach, the Gabor transform indicates the frequency content in localized regions in the spatial domain [6] so that local deviations embedded in a homogeneous pattern can be distinctly identified. In addition, multi-channel Gabor filtering mimics the visual process in the early stage of the human visual system [7, 8]. It is suitable for detecting unexpected and ill-defined anomalies in textured surfaces.

A 2D Gabor function is an oriented complex sinusoidal grating modulated by a 2D Gaussian function [5], which is given by

$$G_{\sigma,f,\theta}(x,y) = g_{\sigma}(x,y) \cdot \exp\left[j2\pi f\left(x\cos\theta + y\sin\theta\right)\right] \tag{1}$$

where

$$g_{\sigma}(x,y) = \frac{1}{2\pi\sigma^{2}} \cdot \exp[-(x^{2}+y^{2})/2\sigma^{2})] \text{ , and } \quad j = \sqrt{-1}$$

The parameters of the Gabor function are specified by the frequency f, the orientation θ of the sinusoid, and the scale σ of the Gaussian function. The 2D Gabor function can be also rewritten as

$$G_{\sigma,u,v}(x\,,\,y) = g_s\,(x\,,\,y)\cdot \exp\left[\mathrm{j}2p\,(ux+vy)\right] \tag{2}$$

where $(u,v) = (f\cos q, f\sin q)$. The norm of the vector gives the frequency f, and the angle of the vector gives the orientation q of the sinusoid. Local orientations and spatial frequencies explicit in Gabor filters are used as the key features for texture processing. In texture discrimination application, the characteristic of each pixel (x, y) in a 2D image is measured by the Gabor-filtered output, which is obtained by the convolution of the image with the 2D Gabor filter $G_{s,u,v}(a\,,b\,)$, i.e.

$$C_{2D}(x,y) = \int_{-\infty}^{\infty}\int_{-\infty}^{\infty} f\,(x+a\,,y+b\,)\cdot G_{s,u,v}(a\,,b\,)d\,adb\;,\quad \forall(x,y) \tag{3}$$

Gabor-filter based methods have been widely applied to texture segmentation [9-12]. The task of defect detection in homogeneously textured surfaces is clearly different from that of texture segmentation since there is no *priori* knowledge on unpredictable defects and they exhibit no distinct textural properties. Two main methods have been proposed in the literature to select proper Gabor filters for texture analysis, the filter-bank approach and the filter-design approach [13]. In filter-bank approaches [6, 14, 15], the filter parameters are present *ad hoc* and are not necessarily optimal for a particular processing task. The input image is generally filtered with a family of Gabor filters tuned to several resolutions and orientations. Clausi and Jernigan [16] compared various Gabor filter implementations for texture analysis. They found that using the Gabor filter magnitude response given a frequency bandwidth and spacing of one octave and orientation bandwidth and spacing of 30 degrees generated preferred results. The filter-bank approaches are not computationally convenient or feasible since they must apply a large number of filters responding at multiple resolutions and orientations to a given image.

In filter-design approaches [4, 11, 13, 17], only one or a few filters for a particular application are designed in an effort to reduce the difficulties of filter-bank approaches. The selection of best filters is generally based on a *priori* knowledge of the texture properties derived from a spectral Fourier analysis of the whole image. The filter-bank and filter-design approaches of 2D Gabor filters have been applied to the inspection of industrial materials such as wineglass [18], steel surfaces [19], wooden surfaces [20], and textile fabrics [21-23].

Tsai and We [24] have considered the issue of designing a single 2D Gabor filter to detect any unpredictable defects in a textured surface. In their algorithm, the design objective for the best Gabor filter is based on the minimization principle that finds the minimum output response of a homogeneous texture pattern in the training process. By defining a non-negative output response, each homogeneous texture region enveloped in a small 2D window will have output amplitude approximate to zero, and any untrained defect region will have distinct output amplitude. The statistical process control principle is then used to set up the control limit (threshold) of output amplitude for distinguishing between defective regions and homogeneous regions in the filter image. Their method has performed well for a variety of real texture samples including textile fabrics, milled surfaces, wood, leather and sandpaper.

Although the 2D Gabor filtering schemes have been widely used for the inspection of industrial materials, rotation-dependency and intensive computation are two inherent problems of 2D Gabor filtering in practical implementation. As seen in Eq. (1), the designed Gabor filter with specific parameter value of orientation q is only used to generate desired output response for a given texture with specific oriented structure. When the oriented texture is rotated in an image, the designed 2D Gabor filter is no longer applicable to describe the textural characteristics. Therefore, the image orientation of a structural texture must be fixed or be predetermined before the use of traditional 2D Gabor filtering methods. Furthermore, for a 2D input image of size $N \times N$, and a 2D Gabor filter of limited size $W \times W$, the computational complexity of traditional 2D Gabor filtering is in the order of $W^2 \cdot N^2$, given that the image orientation is fixed at a specific angle.

In this study, we propose a 1D ring-projection representation and 1D Gabor filtering scheme to improve the method of Tsai and Wu [24] for defect detection in both structural and statistical textures. In order to make the Gabor output response insensitive to image orientation, we first propose a rotation-invariant representation of the 2D gray-level image based on the ring-projection transformation. Ring-projection representation converts the original 2D gray-level image contained in a circular window into a 1D signal as a function of radius. The projection is constructed along concentric rings of increasing radii, and the feature of each ring with a specific radius is represented by the mean gray level of all pixels falling on the ring. The ring-projection representation not only is rotation-invariant but also reduces the data dimensionality for fast computation. Once the 1D ring-projection pattern is obtained, the 1D Gabor filter, instead of the 2D Gabor filter, can be used to efficiently compute the output response of each pixel in the textured image. The 1D Gabor filter along with the 1D ring-projection representation makes the Gabor filtering scheme computationally fast and flexible for detecting defects in structural and statistical textures, regardless of orientation changes.

This paper is organized as follows: Section 2 first describes the 1D ring-projection representation for 2D gray-level textured images. Then the 1D Gabor filtering scheme, and the design of the best Gabor filter are presented. Section 3 demonstrates the experimental results for a variety of real textured surfaces including wooden surface, LCD display, machined surface, granite, leather and sandpaper. The effectiveness and efficiency of both 1D and 2D Gabor filtering methods are also compared in this section. This paper is concluded in Section 4.

2. 1D Discriminating Filter Design

2.1 Ring-projection Representation

In order to reduce the computational burden of the 2D convolution (Eq. (3)) and make the Gabor output response invariant to image rotation, a gray level ring-projection transformation is proposed. It transforms a gray-level textured image in the 2D Cartesian space into a rotation-invariant representation in the 1D ring-projection space. The proposed transformation scheme for gray-level textures is inspired by the ring-projection algorithm [25], which is originally developed for character recognition in binary images.

Let the texture pattern be contained in a circular window of radius $W/2$. The radius $W/2$ chosen for the neighborhood window is selected so that the representation of periodicity and self-similarity of a homogeneous texture pattern is sufficient. The self-similarity means that all subimages enveloped in the neighborhood window are considered similar independently of their positions in the whole textured image. Let the input image be $N \times N$ pixels. The ring projection of a subimage $f(x, y)$ defined in the circular window with the center at (x, y) is given as follows. First, $f(x, y)$ in the Cartesian coordinates is transformed to the polar coordinates:

$$x' = r\cos q,$$
$$y' = r\sin q, \quad \forall (x', y') \ni (x'-x)^2 + (y'-y)^2 \le (W/2)^2$$

Hence $f(x', y') = f(r\cos q, r\sin q)$. The ring-projection of the subimage $f(x, y)$ at radius r, denoted by $P_{x,y}(r)$, is defined as the mean gray value of $f(r\cos q, r\sin q)$ at the specific radius r. That is,

$$P_{x,y}(r) = \frac{1}{2pr}\int_0^{2p} f(r\cos q, r\sin q)\,dq$$

Its discrete form is given by

$$P_{x,y}(r) = \frac{1}{n_r}\sum_k f(r\cos q_k, r\sin q_k), \;\; \forall (x, y) \in N \times N \qquad (4)$$

where n_r is the total number of pixels falling on the circle of radius r, $r = 0, 1, 2, \cdots, W/2$. Taking the mean gray value for each specific ring makes the projected values in various ring radii limited to a controlled range and equal importance. Since the projected values are obtained from circular rings, the derived 1D ring-projection pattern is invariant to rotation of its corresponding 2D texture pattern. Furthermore, it reduces the data dimensionality from $p(W/2)^2$ in the 2D Cartesian space to $W/2$ in the 1D ring projection space, where $W/2$ is the radius of the circular window.

The mechanism of ring-projection transformation is demonstrated in Figure1, where the superimposed circles represent the concentric rings of various radii.

Figures 1(a) and 1(b) present an oriented texture in two distinct orientations (vertical and diagonal line patterns). Figures 1(c) and 1(d) show the plots of ring-projected values as a function of radius r. It can be seen from Figure 1 that these two ring-projection plots are approximately identical, regardless of orientation changes.

2.2 The 1D Gabor Filter

Since the 2D textured image is now represented by a 1D ring-projection pattern, we need only to design a 1D Gabor filter for defect detection. Spatially, a 1D Gabor function is a 1D Gaussian modulated sinusoid. That is,

$$G_{s,u}(r) = g_s(r) \cdot \exp[j2pur], \quad r = 0, 1, 2, \cdots, W/2 \tag{5}$$

where

$$g_s(r) = \frac{1}{\sqrt{2p}\, s} \cdot \exp[-\frac{1}{2}(\frac{r}{s})^2]$$

The term $g_s(r)$ is the 1D Gaussian function with scale parameter s. The complex exponential has a spatial frequency of u. The parameters of a 1D Gabor filter are therefore given by the frequency u and the scale s.

The 1D Gabor filter $G_{s,u}(r)$ forms a complex-valued function. Decomposing $G_{s,u}(r)$ into real and imaginary parts gives

$$G_{s,u}(r) = R_{s,u}(r) + j \cdot I_{s,u}(r) \tag{6}$$

where

$$R_{s,u}(r) = g_s(r) \cdot \cos[2pur]$$

$$I_{s,u}(r) = g_s(r) \cdot \sin[2pur]$$

Gabor-filtered output of a ring-projection pattern $P_{x,y}(r)$ at pixel coordinates (x, y) is obtained by the convolution of the 1D ring-projection pattern $P_{x,y}(r)$ with the 1D Gabor filter $G_{s,u}(r)$, i.e.

$$C_{1D}(x, y) = \int_{-\infty}^{\infty} P_{x,y}(r) \cdot G_{s,u}(r) dr \tag{7}$$

The convolution result of $C_{1D}(x, y)$ is also a complex-valued number. Given a circular window of radius $W/2$ with the center at pixel coordinates (x, y) in the textured image, the discrete convolution of ring-projection pattern $P_{x,y}(r)$ with respective real and imaginary parts of the 1D Gabor filter $G_{s,u}(r)$ are

$$G_R(x, y \mid s, u) = \sum_{r=0}^{W/2} P_{x,y}(r) \cdot R_{s,u}(r) \tag{8a}$$

and

$$G_I(x, y \mid s, u) = \sum_{r=0}^{W/2} P_{x,y}(r) \cdot I_{s,u}(r) \tag{8b}$$

Define the energy at pixel coordinates (x, y) in the filter image as the squared modulus of $C_{1D}(x, y)$, i.e.

$$E(x, y \mid s, u) = [G_R(x, y \mid s, u)]^2 + [G_I(x, y \mid s, u)]^2 \tag{9}$$

for $x, y = W/2, W/2+1, \cdots, N - W/2$, where N is the image width, and $W/2$ is the radius of the circular window that defines the neighborhood region of each pixel (x, y). The computational complexity of the proposed 1D Gabor filtering scheme is only $O(W \cdot N^2)$ for textured images in arbitrary orientations, which is significantly reduced from $O(W^2 \cdot N^2)$ of a traditional 2D Gabor filtering method that requires oriented textures in fixed orientations.

Note that the energy defined in Eq. (9) is a non-negative real number. If the Gabor-filter parameters are selected so that the corresponding energy is a minimum for a specific texture sample, every filtered subimage that has a similar texture pattern to the training sample will generate the energy value close to zero. Any subimage with the texture pattern different from the training one will yield a distinctly large energy value. This converts the difficult defect detection problem in complicated textured-surfaces into a simple binary thresholding problem where low energy represents homogeneous textures and high energy represents local anomalies.

In this work, we are considering a supervised inspection problem, i.e. representative samples of the textures of interest are given to help in designing the most discriminating filter. The training sample can be arbitrarily selected from a faultless region of textured surface. The neighborhood window of radius $W/2$ is selected so that the representation of self-similarity of a homogeneous texture pattern is sufficient. For a given training texture T_0 with circular size of radius $W/2$ and center at (x_0, y_0), the optimal Gabor-filter parameters (s, u) are given by

$$Min \quad E(x_0, y_0 \mid s, u)$$

Subject to

$$s_{\min} \le s \le s_{\max} \tag{10a}$$

$$u_{\min} \le u \le u_{\max} \tag{10b}$$

where $E(x_0, y_0 \mid s, u)$ is the energy of the model image T_0, and it can be obtained from Eq. (9). The constraints 10(a) and 10(b) specify the possible ranges of filter parameters s and u. The terms $s_{\min}$ and $s_{\max}$ are the minimum and maximum values of s; $u_{\min}$ and $u_{\max}$ are the minimum and maximum values of

u. We can generally select $s_{\min}$, $u_{\min} = 1$ and $s_{\max}$, $u_{\max} = W/2$.

The formulated model above is a nonlinear optimization problem. This may call for sophisticated optimization techniques such as the simulated annealing (SA) search algorithm [12] to determine the best parameter values of s and u. We have conducted an empirical study to compare the detection results from the exhaustive search with the resolution of 1 for scale parameter s and 0.01 for frequency parameter u, and the SA search method with the resolution of 0.001 for both parameters. The detection results showed that the energy function defined in Eq. (9) is not very sensitive to minor variation of the parameter values. Both exhaustive and SA search methods have performed equally well to generate the objective function value smaller than 0.01. The exhaustive search with the suggested resolution setting can be easily implemented, and computationally simple. For a circular window of radius 30 pixels, the training time can be completed in 10 seconds with a typical personal computer. Since the training process can be carried out off-line, a simple exhaustive search will serve the purpose to find a best parameter set (s, u).

In the inspection process, the selected Gabor filter will slide over the whole sensed image on a pixel-by-pixel basis so that the corresponding energy of every pixel in the image can be determined. The filter will give a minimum energy response close to zero when the sliding window covers a homogeneous texture region in the image, and will generate a large energy response for a defective region. This transforms texture differences into detectable filter output. A simple statistical process control principle proposed in reference [24] can be used to set up the control limit for distinguishing defects from homogeneous textures in the filter image.

3. Experimental results

In this section, we present the experimental results for evaluating the efficacy of the proposed 1D Gabor filtering scheme for defect detection in textured surfaces. All experiments are implemented on a personal computer with a Pentium II-400 Mhz processor using the C language. The algorithm is tested on a number of real textured surfaces including wooden surface, LCD display, milled surface, granite, leather and sandpaper. All input images are 256×256 pixels wide with 8-bit gray-levels. The radius of the circular window ranges between 15 and 30 pixels depending on the texture pattern in question. In the training process, a subimage enveloped in an appropriate circular window is arbitrarily selected from a faultless reference image of each texture class to determine the best filter parameters.

For defect detection in structural textures, Figure 2(a) shows a faultless wooden surface. The square frame in the figure marks the subimage used in training. The radius of the circular window is 30 pixels. Figure 2(b) and 2(c) present a clear wooden surface and a defective one used in the inspection process. Figures 2(d) and 2(e) depict the respective plots of the energy function in 3D perspective for Figures 2(b) and 2(c). Figure 2(f) further shows the output energy as an intensity function for Figure 2(c), where brightness is proportional to the magnitude of energy. Figures 2(d)-(f) show that the energy values are small and uniformly distributed in the filter image for a clear wooden surface, whereas the energy values of pixels in the irregular region for a defective wooden surface are distinctly large.

Figure 3(a) shows a faultless LCD display, in which the white square frame marks the training subimage. The radius of the circular window is 15 pixels.

Figures 3(b) and 3(c) present a clear LCD display, and a defective LCD display with hardly visible scratches. It can be observed from the corresponding detection results in Figures 3(d)-(f) that the proposed 1D Gabor-filter detector can also identify the scratches even though they are subtle defects in the LCD display.

For defect detection in statistical textures, Figure 4(a) shows a faultless granite image with randomly textured surface. The white square frame on the upper left of the figure marks the training subimage. The radius of the circular window is only 15 pixels. Figures 4(b) and 4(c) present a clear granite surface and a defective one used in the inspection process. Figures 4(d)-(f) illustrate the corresponding detection results, which show that all pixels in the homogeneous texture regions have small energy values close to zero, and pixels in the defective regions have notably large energy values. Table 1 summarizes the selected Gabor parameter values and the resulting energy values for the training samples shown in Figures 2(a), 3(a) and 4(a). Note that all trained energy values are approximately equal to zero.

In the proposed method, the radius of neighborhood window affects the inspection results. The choice of a proper circular window size must be large enough to contain the periodic, repetitive pattern of a homogeneous texture in question. Too small a window size causes insufficient representation of texture information, whereas too large a window size increases the computational burden. Figure 5(a) presents a structural texture of paper surface with a contamination defect. Figures 5(b) and 5(c) show the resulting energy values as an intensity function from the circular windows of radii 15 and 20 pixels, respectively. Figure 6(a) shows a statistical texture of leather surface with a wear defect. The corresponding detection results from the circular windows of radii 20 and 30 pixels are presented in Figures

6(b) and 6(c). Figures 5 and 6 reveal that the detected number of high-energy pixels in the defective regions becomes small and distributes more scatteringly for an undersized window. For a sufficiently large window size, the high-energy pixels associated with the defective regions in the textured image are significant and well separated in the resulting filter image. Our empirical study on a numerous texture samples has shown that the circular window of radius 30 pixels is generally sufficient for defect detection applications. In practical implementation, the choice of a window radius in the range between 25 and 35 pixels is suggested for the trade-off between detection effectiveness and computational efficiency.

In order to evaluate the effect of rotation changes on detection results, Figures 7(a1), (b1) and (c1) show a defective wooden surface in 0°- (vertical lines), 40°- (approximately diagonal lines) and 80°- (approximately horizontal lines) orientations. The faultless wooden surface shown in Figure 2(a) is used as the reference texture in training. Figures 7(a2), (b2) and (c2) present the resulting energy values as an intensity function using the proposed 1D Gabor filtering scheme. They show that the proposed method is invariant to orientation changes for structural textures with highly oriented patterns. All defects in Figures 7(a1)-(c1) are reliably detected, regardless of image orientations. Figures 7(a3), (b3) and (c3) show the corresponding detection results as an intensity function using the 2D Gabor filtering method. The results reveal that the defect can be well detected if the orientation of the texture under inspection is coincident with the training one, as shown in Figure 7(a3). However, the 2D Gabor filtering method performs poorly for the texture in different orientations, as seen in Figures 7(b3) and 7(c3).

Finally, we compare the differences of output responses in the filter image between the 1D and 2D Gabor filtering methods. Figures 8(a) and 9(a) show respectively a milled surface (structural texture) with a scratch defect, and a sandpaper surface (statistical texture) with a wear defect. The resulting output energies from the 1D and 2D Gabor filtering methods are depicted as an intensity function, as seen in Figures 8(b)-(c) and Figure 9(b)-9(c), and are plotted in 3D perspective, as seen in Figures 8(d)-(e) and Figures 9(d)-(e). It can be seen from both Figures 8 and 9 that the detected defective elements from the 2D Gabor filtering method are highly concentrated, whereas the detected defective elements from the 1D Gabor filtering scheme are more scattering. In terms of resultant energy values, both 1D and 2D Gabor filtering methods generate distinctly high output responses for defective regions in the filter image, as seen in the 3D plots of Figures 8(d)-(e) and 9(d)-(e).

Table 2 summarizes the computation times of the 1D and 2D Gabor filtering methods for various window radii. The computation time is based on an input image of size 256×256 with a Pentium II-400 Mhz personal computer. As shown in Table 2, the inspection time of the proposed 1D Gabor filtering scheme is only 0.7 seconds for a large window of radius 32 pixels, compared to 165 seconds of the 2D Gabor filtering method. The proposed 1D Gabor filtering method is far more efficient than the 2D one.

4. Conclusions

Detecting small defects which appear as local anomalies embedded in a homogeneously textured surface is a common problem in industrial inspection. The traditional 2D Gabor filtering methods have shown to be an effective technique for automatic surface inspection. However, they suffer from the inherent properties of rotation-dependency and intensive computation, and become impractical for on-line inspection applications.

In this paper, we have proposed a fast rotation-invariant defect detection method that incorporates the 1D ring projection representation and the 1D Gabor filtering to alleviate the limitations of the 2D Gabor filtering methods. The 2D circular subimage in a textured image is first transformed to a 1D pattern in the ring-projection space. The ring-projection representation not only eases the computational complexity by reducing the data dimensionality, but also makes the detection invariant to rotation. Then a 1D Gabor filter is used to compute the output response by convoluting each circular subimage with the Gabor filter in a pixel-by-pixel basis throughout the whole input image. Pixels in the homogeneous region will have small output amplitude approximate to zero, and pixels in any defective region will yield distinctly high output amplitude.

Experimental results have shown that the proposed 1D Gabor filtering scheme is very efficient in computation and effective in detection for both structural textures such as textile fabric, machined surface, wooden surface and LCD display, and statistical textures such as sandpaper, leather and granite. The proposed method is not affected by rotation changes for structural textures with highly oriented patterns. The detected defect size from the 1D Gaobr filtering scheme is relatively scattering, and the one from the 2D Gabor filtering method is highly concentrated. Both 1D and 2D Gabor filtering methods generate high-energy values for defective regions, which are distinctly discriminate from the uniformly small energy values for homogeneous regions in the filter image. Due to the computational efficiency of the proposed 1D Gabor filtering scheme, on-line defect detection in textured surfaces can be realized.

References

1. A. Pikaz and A. Averbuch, "An efficient topological characterization of gray-levels textures using a multiresolution representation," *Graphical Models and Image Processing*, 59, pp. 1-17, 1997.

2. T. S. Newan and A. K. Jain, "A survey of automated visual inspection," *Computer Vision and Image Understanding*, 61, pp. 231-262, 1995.

3. M. Porat and Y. Y. Zeevi, "The generalized Gabor scheme of image representation in biological and machine vision," *IEEE Transactions on Pattern Analysis and Machine Intelligence*, 10, pp. 452-468, 1988.

4. A. C. Bovik, M. Clark and W. S. Geisler, "Multichannel texture analysis using localized spatial filters," *IEEE Transactions on Pattern Analysis and Machine Intelligence*, 12, pp. 55-73, 1990.

5. J. G. Daugman, "Uncertainty relation for resolution in space, spatial-frequency and orientation optimized by two-dimensional visual cortical filters," *Journal of the Optical Society of America*, 2, pp. 1160-1169, 1985.

6. T. R. Reed and H. Wechsler, "Segmentation of textured images and Gestalt organization using spatial/spatial-frequency representations," *IEEE Transactions on Pattern Analysis and Machine Intelligence*, 12, pp. 1-12, 1990.

7. R. L. De Valois, D. G. Albrecht and L. G. Thorell, "Spatial frequency selectivity of cells in macaque visual cortex," *Vision Research*, 22, pp. 545-559, 1982.

8. J. Beck, A. Sutter and R. Ivry, "Spatial frequency channels and perceptual grouping in texture segregation," *Computer Vision, Graphics and Image Processing*, 37, pp.

299-325, 1987.

9. M. Clark and A. C. Bovik, "Texture segmentation using Gabor modulation/demodulation," *Pattern Recognition Letters*, 6, pp. 261-267, 1987.

10. D. Dunn and W. E. Higgins, "Optimal Gabor filters for texture segmentation," *IEEE Transactions on Image Processing*, 4, pp. 947-964, 1995.

11. T. P. Weldon, W. E. Higgins and D. F. Dunn, "Efficient Gabor filter design for texture segmentation," *Pattern Recognition*, 29, pp. 2005-2015, 1996.

12. D. –M. Tsai, S. –K. Wu and M. –C. Chen, "Optimal Gabor filter design for texture segmentation using stochastic optimization," *Image and Vision Computing*, 19, pp. 299-316, 2001.

13. T. P. Weldon, W. E. Higgins and D. F. Dunn, "Gabor filter design for multiple texture segmentation," *Optical Engineering*, 35, pp. 2852-2863, 1996.

14. A. K. Jain and F. Farrokhnia, "Unsupervised texture segmentation using Gabor filters," *Pattern Recognition*, 24, pp. 1167-1186, 1991.

15. P. P. Raghu and B. Yegnanarayana, "Segmentation of Gabor-filtered textures using deterministic relaxation," *IEEE Transactions on Image Processing*, 5, pp. 1625-1636, 1996.

16. D. A. Clausi and M. E. Jernigan, "Designing Gabor filters for optimal texture separability," *Pattern Recognition*, 32, pp. 1835-1849, 2000.

17. A. C. Bovik, "Analysis of multichannel narrow-band filters for image texture segmentation," *IEEE Transactions on Signal Processing*, 39, pp. 2025-2043, 1991.

18. J. Wang and A. K. Asundi, "Computer vision system for wineglass defect

inspection via Gabor-filter-based texture features," *Information Sciences*, 127, pp. 157-171, 2000.

19. K. Wiltschi, A. Pinz and T. Lindeberg, "Automatic assessment scheme for steel quality inspection," *Machine Vision and Applications*, 12, pp. 113-128, 2000.

20. W. Polzleitner and G. Schwingskakl, "Quality classification of wooden surfaces using Gabor filters and genetic feature optimization," *Proceedings of SPIE*, 3837, pp. 220-231, 1999.

21. J. Escofet, R. B. Navarro, M. S. Millan and J. M. Pladellorens, "Detection of local defects in textile webs using Gabor filters," *Proceedings of SPIE*, 2785, pp. 163-170, 1996.

22. A. Bodnarova, M. Bennamoun and S. J. Latham, "Constrained minimisation approach to optimise Gabor filters for detecting flaws in woven textiles," *Proceedings of the IEEE International Conference on Acoustics, Speech and Signal Processing*, 6, pp. 3606-3609, 2000.

23. A. Kumar and G. Pang, "Defect detection in textured materials using Gabor filters," *Conference Record-IAS Annual Meeting, IEEE Industry Applications Society*, 2, pp. 1041-1047, 2000.

24. D. –M. Tsai and S. –K. Wu, "Automated surface inspection using Gabor filters," *International Journal of Advanced Manufacturing Technology*, 16, pp. 474-482, 2000.

25. Y. Y. Tang, H. D. Cheng and C. Y. Suen, "Transformation-ring-projection (TRP) algorithm and its VLSI implementation," *International Journal of Pattern Recognition and Artificial Intelligence*, 5, pp. 25-56, 1991.

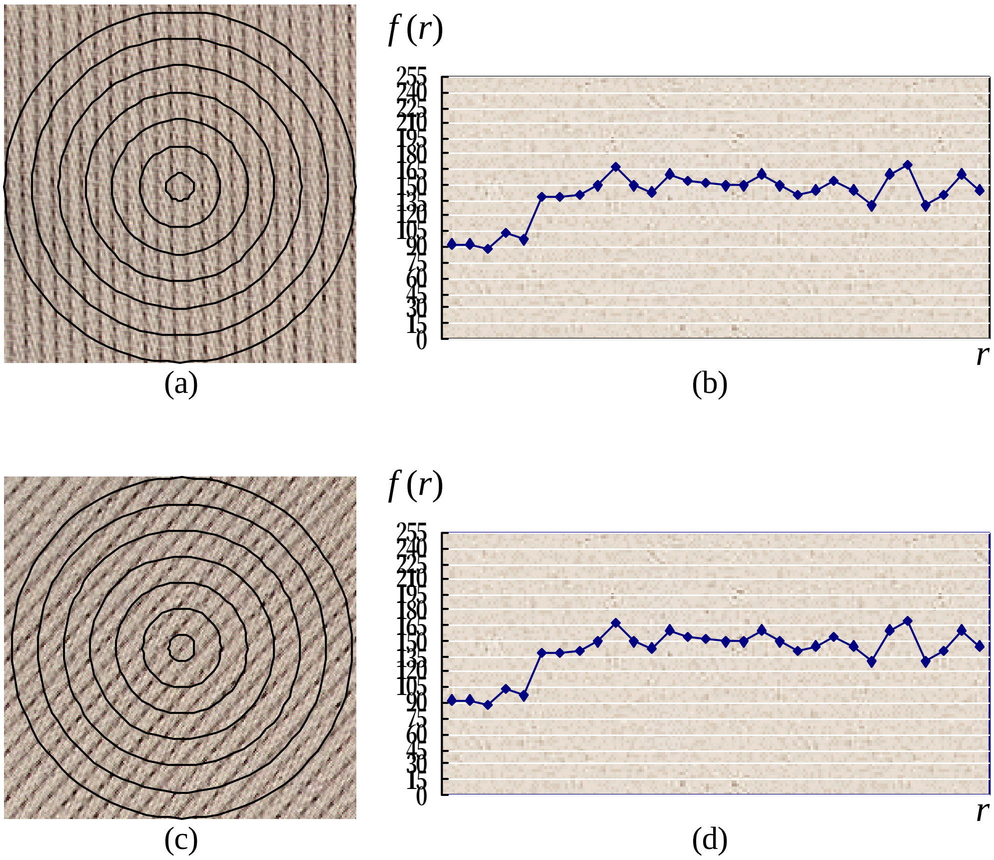

Figure 1. An oriented fabric texture in two different orientations. (a) and (b) The original images. (c) and (d) The respective ring-projection plots.

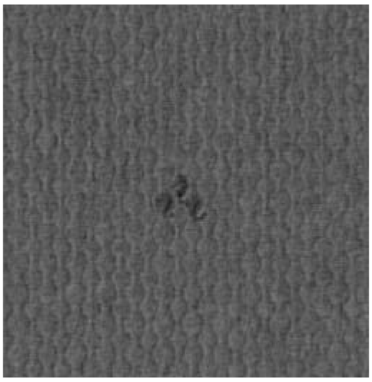

(a)

(b)

(c)

Figure 2. The effect of the window size for a structural texture. (a) The test sample of a paper surface. (b) and (c) The respective detection results from windows of radii 15 and 20 pixels.

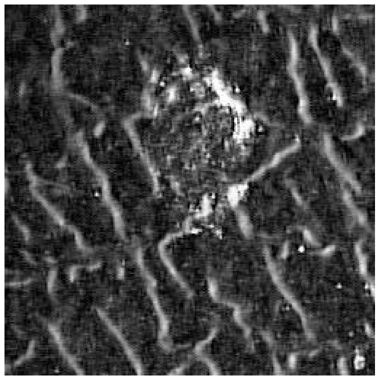

(a)

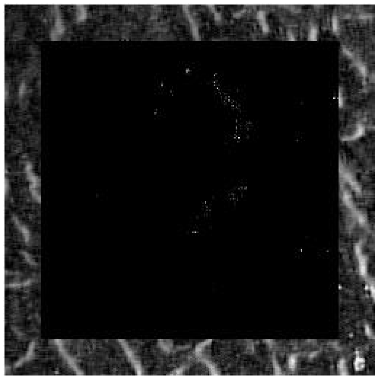

(b)

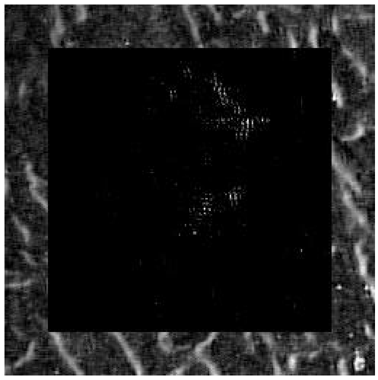

(c)

Figure 3. The effect of the window size for a statistical texture. (a) The test sample of a leather surface. (b) and (c) The respective detection results from windows of radii 20 and 30 pixels.

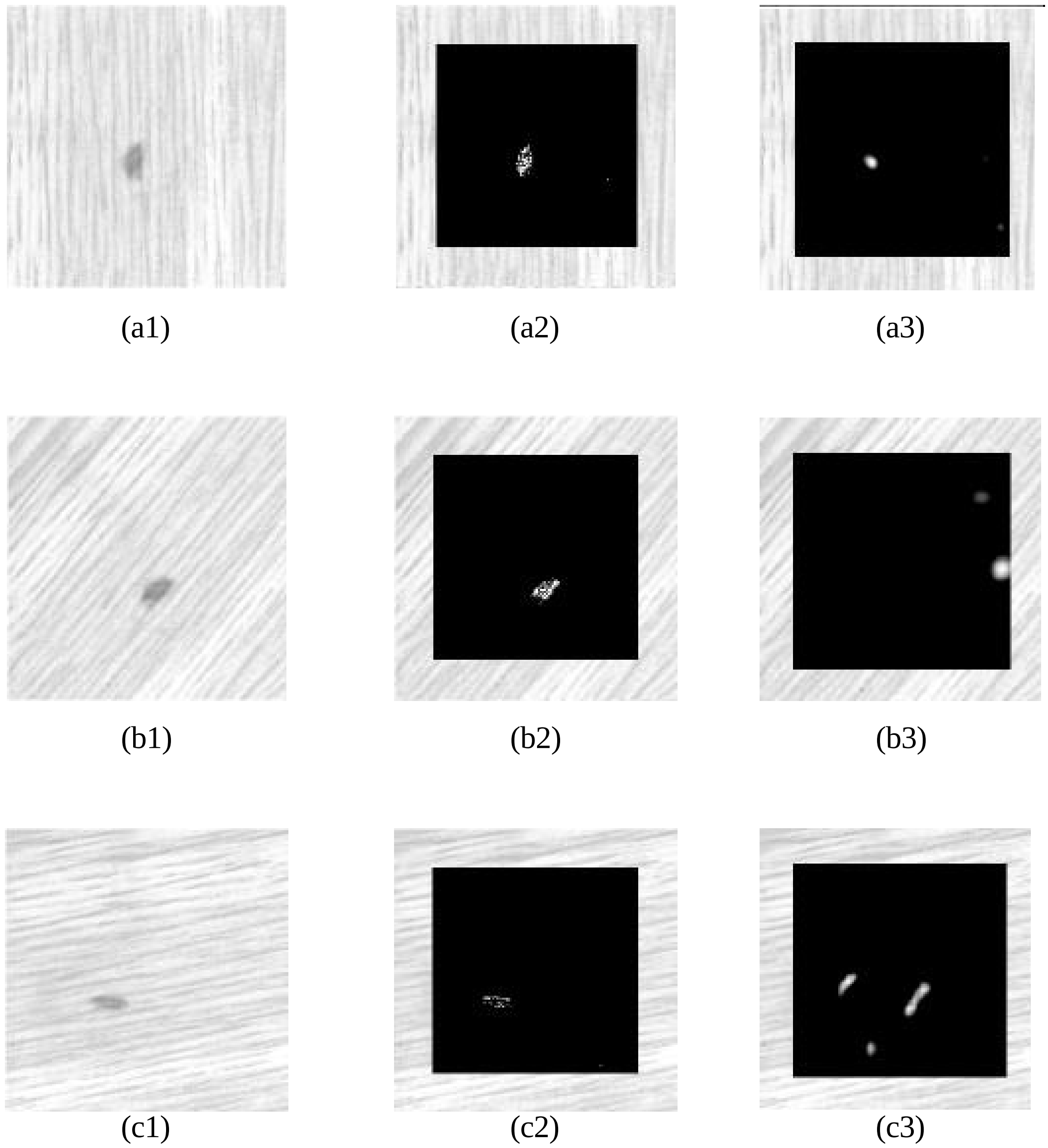

Figure 4. The effect of changes in image rotation. (a1), (b1) and (c1) The defective wooden surface in three different orientations. (a2), (b2) and (c2) The respective detection results from the proposed 1D Gabor filtering scheme. (a3), (b3) and (c3) The respective detection results from the 2D Gabor filtering method.

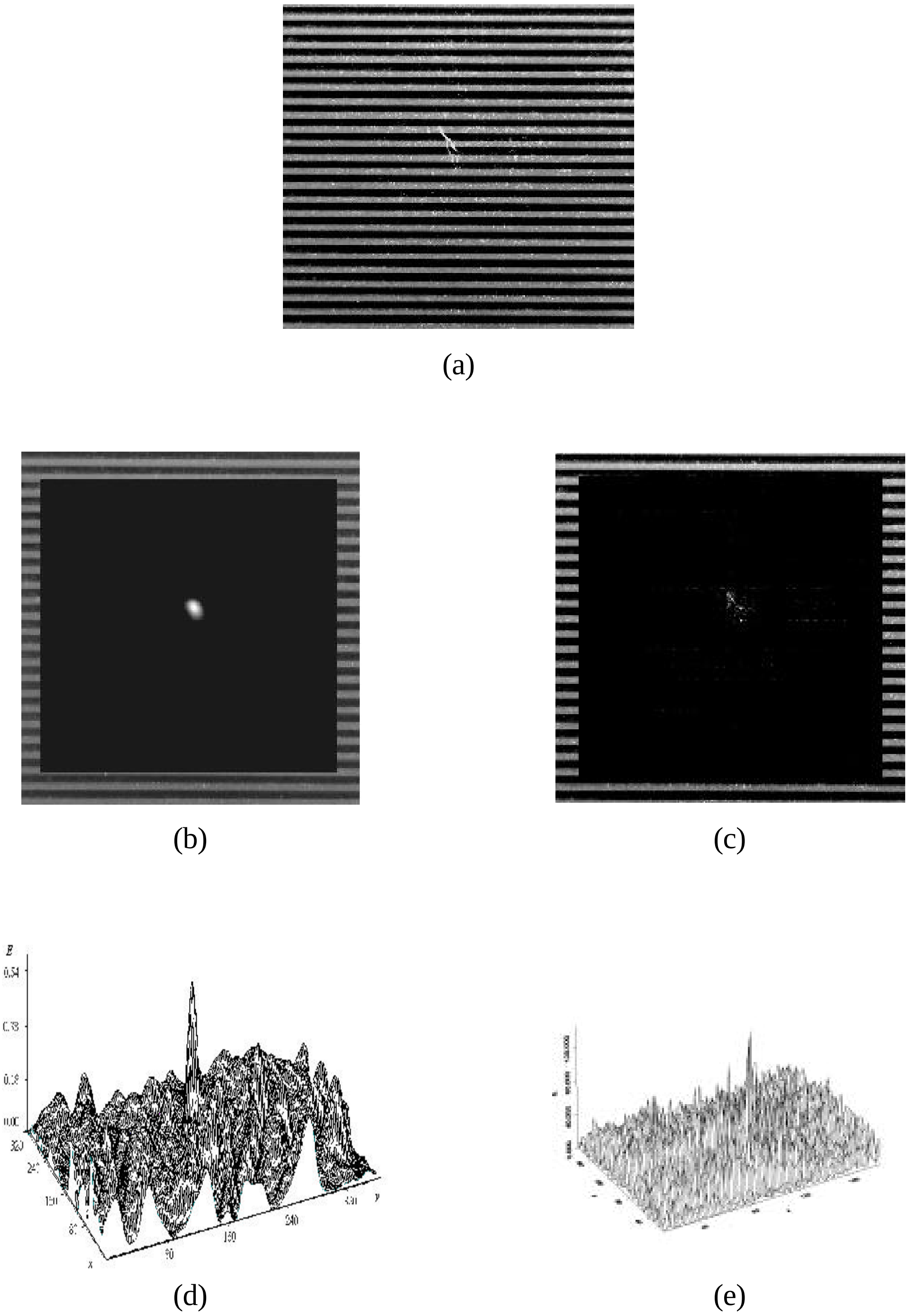

Figure 5. A comparison of detection results for a structural texture using the 1D and 2D Gabor filtering methods. (a) The original image of a milled surface. (b) and (c) The respective visual displays of the energy as an intensity function. (d) and (e) The respective energy functions in 3D perspective.

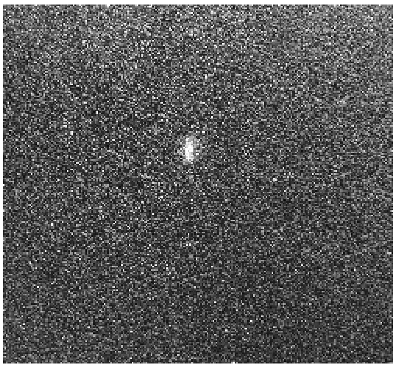

(a)

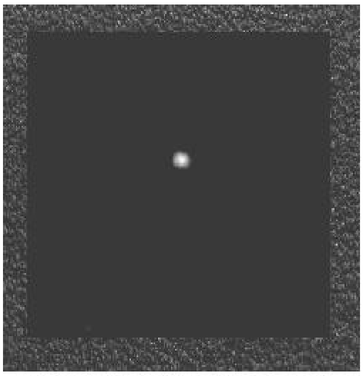

(b)

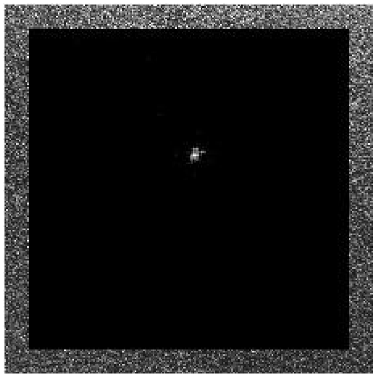

(c)

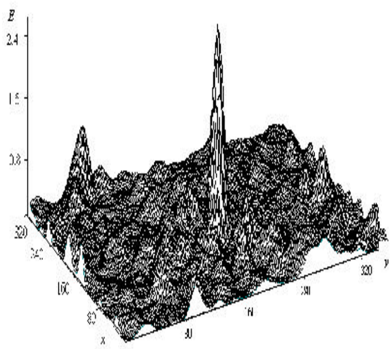

(d)

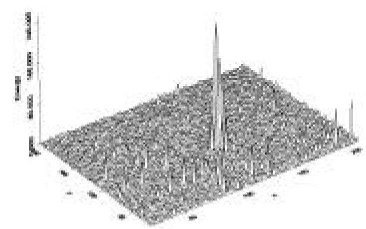

(e)

Figure 6. A comparison of detection results for a statistical texture using the 1D and 2D Gabor filtering methods. (a) The original image of a sandpaper surface. (b) and (c) The respective visual displays of the energy as an intensity function. (d) and (e) The respective energy functions in 3D perspective.

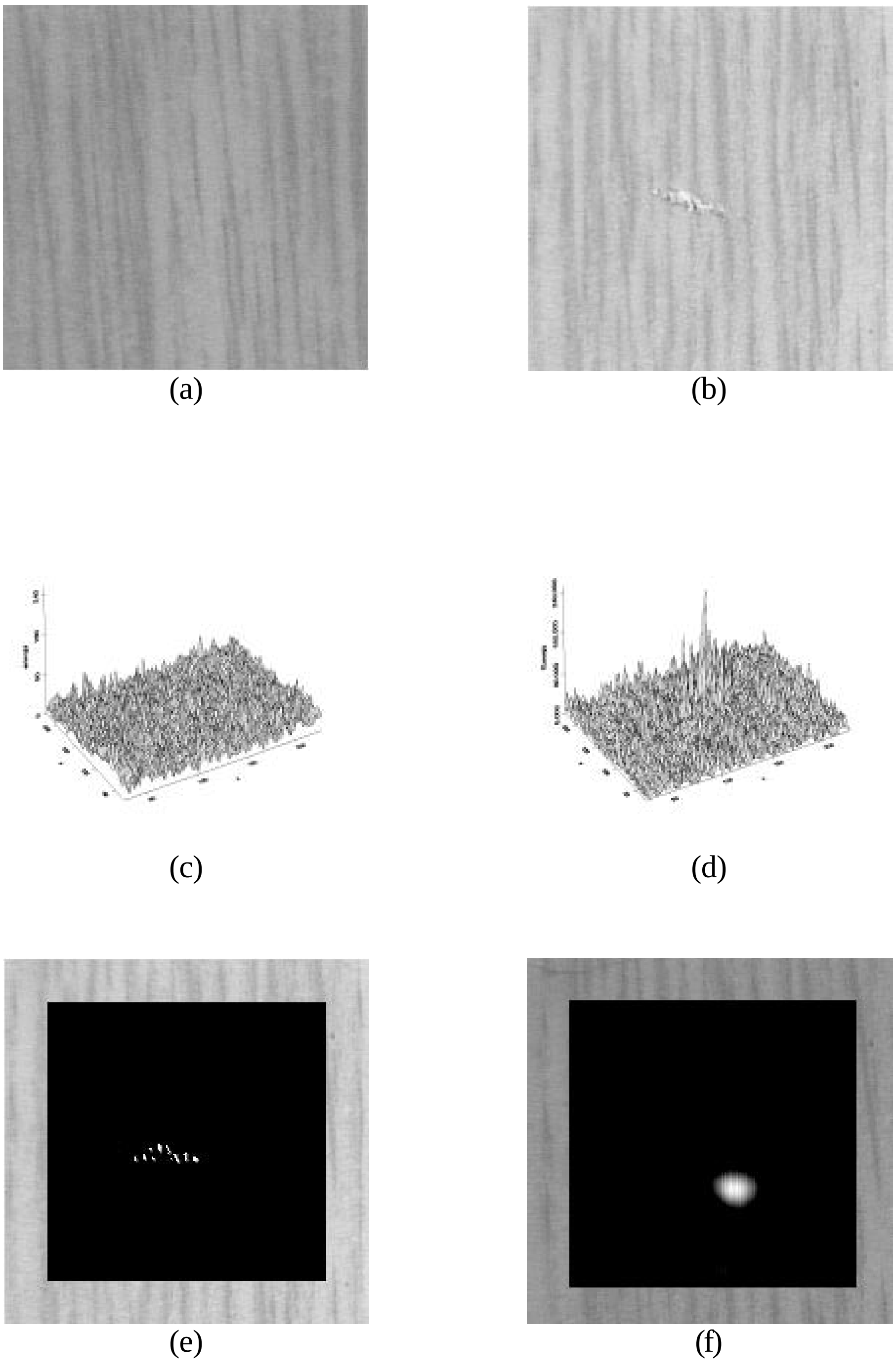

Figure 7. (a). A clear wooden surface. (b) A defective wooden surface. (c) and (d) The respective energy functions in 3D perspective for (a) and (b). (e) and (f) The respective detection results of the energy as an intensity function for (b) from the 1D and 2D Gabor filtering methods.

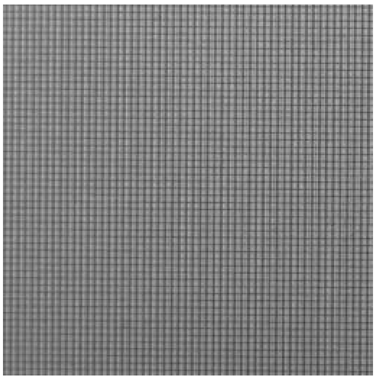

(a)

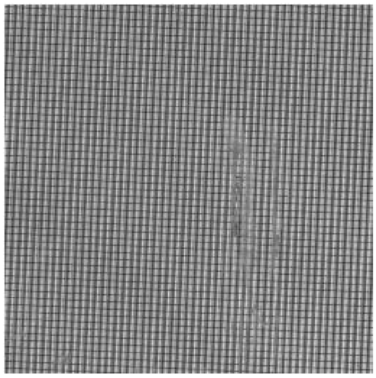

(b)

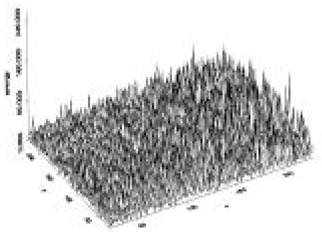

(c)

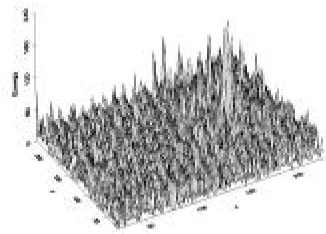

(d)

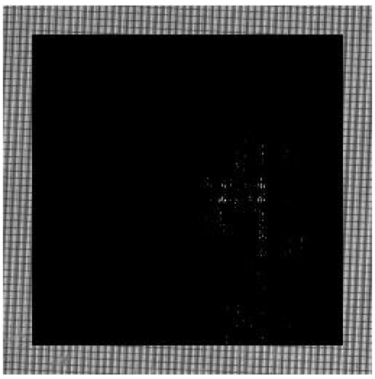

(e)

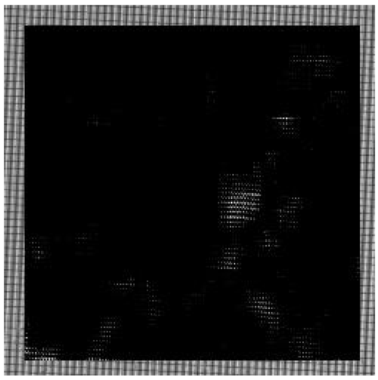

(f)

Figure 8. (a) A clear LCD surface. (b) A defective LCD surface with scratches. (c) and (d) The respective energy functions in 3D perspective for (b) and (c). (e) and (f) The respective detection results from the 1D and 2D Gabor filtering methods for the defective sample in (b).

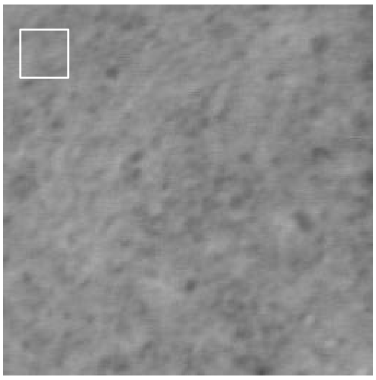

(a)

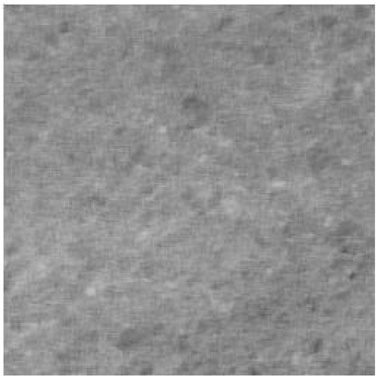

(b)

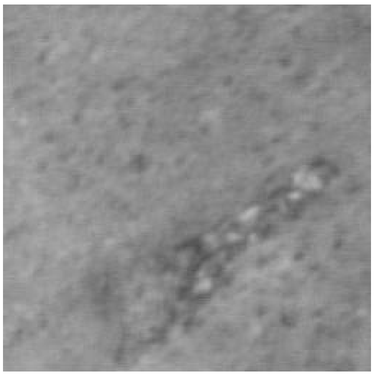

(c)

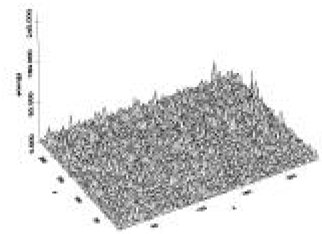

(d)

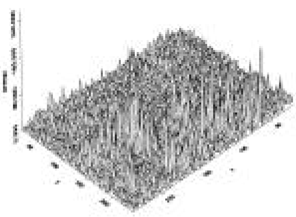

(e)

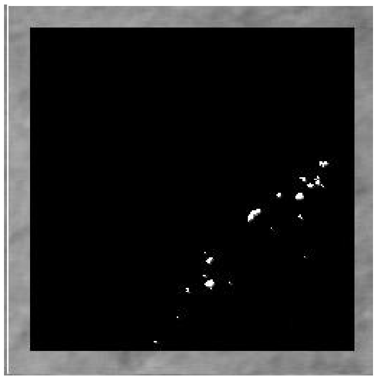

(f)

Figure 9. (a) A faultless granite surface used in training. (b) A clear granite surface. (c) A defective granite surface. (d) and (e) The respective energy functions in 3D perspective for (b) and (c). (f) The resulting energy values as an intensity function for the defective granite in (c).

Table 1. The comparison of computation times with the 1D and 2D Gabor filtering methods.

Window size		Training time (sec.)		Inspection time (sec.)	
2D Gabor ($W \times W$)	1D Gabor ($W/2$)	2D Gabor	1D Gabor	2D Gabor	1D Gabor
25×25	12	220	2	65	0.4
41×41	20	340	4	93	0.5
51×51	25	455	6	116	0.6
65×65	32	585	12	165	0.7

* Based on an input image of 256×256 pixels and a Pentium II-400 MHz PC.

Table 2. The trained energy values and filter parameter values.

Textured image		Energy E	Filter parameters (s, u)
Wood	(Fig. 7(a))	0.000052	(25 , 24.75)
LCD	(Fig. 8(a))	0.000865	(15 , 10.40)
Granite	(Fig. 9(a))	0.004986	(20 , 1.59)